12th International Conference on CFD in Oil & Gas, Metallurgical and Process Industries
SINTEF, Trondheim, NORWAY
May 30th - June 1st, 2017

INFLUENCE OF THE UPSTREAM CYLINDER AND WAVE BREAKING POINT ON THE BREAKING WAVE FORCES ON THE DOWNSTREAM CYLINDER

Arun KAMATH[1*], **Mayilvahanan ALAGAN CHELLA**[1†], **Hans BIHS**[1‡], **Øivind A. ARNTSEN**[1§]

[1]NTNU Department of Civil and Transport Engineering, 7491 Trondheim, NORWAY

[*] E-mail: arun.kamath@ntnu.no
[†] E-mail: acm@ntnu.no
[‡] E-mail: hans.bihs@ntnu.no
[§] E-mail: oivind.arntsen@ntnu.no

ABSTRACT

The interaction of breaking waves with marine structures involves complex free surface deformation and instantaneous loading on the structural members. A typical offshore platform or a coastal structure consists of several vertical and horizontal members exposed to breaking wave action. The breaking wave hydrodynamics and the effect of neighbouring cylinders on multiple cylinders placed in near vicinity is important due to force amplification or reduction resulting from interaction between the cylinders. The kinematics of breaking waves and the hydrodynamics of breaking wave interaction with a single vertical cylinder have been studied in detail in current literature. Studies have established that the location of a cylinder with respect to the wave breaking point has a major influence on the breaking wave forces on the cylinder. These studies have to be extended to investigate the hydrodynamics of cylinders placed close to each other to understand the modifications in the force regime due to the presence of neighbouring cylinders under a breaking wave regime.

In this paper, the open-source Computational Fluid Dynamics (CFD) model REEF3D is used to simulate breaking wave interaction with a pair of tandem cylinders. The focus of the study is on the location of the wave breaking point with respect to the upstream cylinder and the consequences for the downstream cylinder. The free surface features associated with the incident breaking wave and the evolution of the free surface after interaction with the upstream cylinder are investigated. The overturning wave crest and the associated free surface deformation have a major influence on the wave that is then incident on the downstream cylinder. The development of a downstream jet behind the upstream cylinder leads to the negation of the shadowing effect on the downstream cylinder. This can lead to an unexpected higher force on the downstream cylinder. The evolution of this downstream jet and the extent of this phenomenon changes the character of the otherwise shadow region behind the upstream cylinder. A detailed understanding of this phenomenon can provide new insights into the wave hydrodynamics related to multiple cylinders placed in close vicinity under a breaking wave regime. The knowledge regarding force amplification or reduction on downstream cylinders will aid in designing a safer and reliable substructure for marine installations.

Keywords: CFD, hydrodynamics, breaking wave, wave force, tandem cylinders .

NOMENCLATURE

Greek Symbols

Γ	Relaxation function, []
ρ	Fluid density, $[kg/m^3]$
ν	Kinematic viscosity, $[m^2/s]$
ν_t	Eddy viscosity, $[m^2/s]$
ω	Specific turbulent dissipation rate, $[1/s]$
Ω	Surface of object, $[m^2]$
$\phi(\vec{x},t)$	Level set function, $[m]$
η	Free surface elevation, $[m]$
τ	viscous shear stress tensor, $[N/m^2]$

Latin Symbols

d	still water level, $[m]$.
p	Pressure, $[Pa]$.
g	Acceleration due to gravity, $[m/s^2]$.
D	Cylinder diameter, $[m]$.
F	Total force, $[N]$.
H	Wave height, $[m]$.
S	centre to centre separation distance between the cylinders, $[m]$.
T	Wave period, $[s]$.
U	time-averaged velocity, $[m/s]$.

Sub/superscripts

i	Index i.
j	Index j.

INTRODUCTION

Simulating the propagation and interaction of breaking waves produced by reducing water depth presents challenges due to the complex physical processes involved, with highly non-linear interactions and rapid variations in the free surface. Several numerical investigations have attempted to model wave breaking over plane slopes such as Lin and Liu (1998); Zhao *et al.* (2004); ALAGAN CHELLA *et al.* (2015a). With the help of these studies, detailed information about breaking wave characteristics and the geometric properties of breaking waves under different incident conditions and bottom slope have been obtained. The empirical coefficients used for the evaluation of breaking wave forces in other structural models and design considerations are determined using the breaking wave parameters quantified by these studies. With the advances in computational modelling and with the establishment of CFD models that can represent the breaking process in a satisfactory manner, breaking wave forces on structures can be calculated. In current literature, Bredmose and Jacobsen (2010) present breaking

wave impact forces due to focussed waves with the JoNSWAP wave spectrum for input and carried out computations for half the domain assuming lateral symmetry of the problem using OpenFOAM. Mo *et al.* (2013) measured and modelled solitary wave breaking and its interaction with a slender cylinder over a plane slope for a single case using the filtered Navier-Stokes equations with large eddy simulation (LES) turbulence modelling. Choi *et al.* (2015) investigated breaking wave impact forces on a vertical cylinder and two cases of inclined cylinders for one incident wave using the modified Navier-Stokes equations with the volume of fluid (VOF) method for interface capturing to study the dynamic amplification factor due to structural response. These investigations present results for breaking wave interaction with a single cylinder, while breaking wave forces on tandem cylinders, the effect of neighbouring cylinders on the breaking wave forces on the cylinders along with the complex free surface deformations associated with the interaction are not presented in detail.

In the current study, the open source CFD model REEF3D (Bihs *et al.*, 2016) is used to simulate periodic breaking wave forces on tandem cylinders in a three-dimensional wave tank without assuming lateral symmetry. The model has been previously used to simulate the wave breaking process under different conditions (ALAGAN CHELLA *et al.*, 2015b,c) and the wave breaking kinematics were fully represented including the motion of the jet, air pocket formation and the reconnection of the jet with the preceding wave trough. Following the work presented in (Kamath *et al.*, 2016), the effect of breaker location and the upstream cylinder on the wave forces on a second cylinder placed downstream in tandem is investigated.

MODEL DESCRIPTION

Governing Equations

In the numerical wave tank REEF3D, the incompressible three-dimensional Reynolds-Averaged Navier-Stokes (RANS) equations are solved in conjunction with the continuity equation:

$$\frac{\partial U_i}{\partial x_i} = 0 \tag{1}$$

$$\frac{\partial U_i}{\partial t} + U_j \frac{\partial U_i}{\partial x_j} = -\frac{1}{\rho}\frac{\partial p}{\partial x_i} + \frac{\partial}{\partial x_j}\left[(\nu + \nu_t)\left(\frac{\partial U_i}{\partial x_j} + \frac{\partial U_j}{\partial x_i}\right)\right] + g_i \tag{2}$$

where U is the velocity, ρ is the density of the fluid, p is the pressure, ν is the kinematic viscosity, ν_t is the eddy viscosity and g the acceleration due to gravity.

Discretisation Schemes

The convective terms of the RANS equations are discretised using the fifth-order conservative finite difference Weighted Essentially Non-Oscillatory (WENO) scheme (Jiang and Shu, 1996) and time advancement is carried out using a Total Variation Diminishing (TVD) third-order Runge-Kutta explicit time scheme (Shu and Osher, 1988). The CFL criterion is used in an adaptive time stepping algorithm to determine the optimal time step for each step in the simulation. An implicit time scheme is used for diffusion to remove it from the CFL criterion. The projection method (Chorin, 1968) is applied for pressure treatment and the Poisson pressure equation is solved with a PFMG preconditioned (Ashby and Flagout, 1996) BiCGStab solver (van der Vorst, 1992) from the high performance solver library HYPRE (hyp, 2015). The code is parallelised using the MPI (Message Passing Interface) framework. A staggered Cartesian grid is employed in the model and complex geometries are accounted for using the ghost cell immersed boundary method

Free surface and Turbulence modelling

The two equation k-ω model is employed for turbulence closure (Wilcox, 1994) along with eddy viscosity limiters (Durbin, 2009) and a free surface turbulence damping scheme (Naot and Rodi, 1982). The hydrodynamics are modelled in a two-phase flow approach, calculating the flow for both water and air. The level set method (Osher and Sethian, 1988) captures the interface between the two fluids. (Berthelsen and Faltinsen, 2008). Further details regarding the numerical model REEF3D can be obtained in Bihs *et al.* (2016).

Numerical Wave Tank

The numerical model is used as a numerical wave tank to model and calculate wave hydrodynamics. Waves are generated on one end of the tank using the relaxation method (Larsen and Dancy, 1983) with the relaxation functions presented by Jacobsen *et al.* (2012). The velocity and the free surface in the relaxation generation zone is modulated as follows:

$$\begin{aligned} U_{relaxed} &= \Gamma(x) u_{analytical} + (1-\Gamma(x)) u_{computational} \\ \phi_{relaxed} &= \Gamma(x) \phi_{analytical} + (1-\Gamma(x)) \phi_{computational} \end{aligned} \tag{3}$$

where $\Gamma(x)$ is a relaxation function and $x \in [0,1]$ is the x-coordinate scaled to the length of the relaxation zone. The relaxation function shown in Eq. (4) is used in the current numerical model (Jacobsen *et al.*, 2012):

$$\Gamma(x) = 1 - \frac{e^{(1-x)^{3.5}} - 1}{e-1} \tag{4}$$

The generation zone is generally one wavelength long and is not considered an active part of the numerical wave tank. A similar relaxation zone can be defined to absorb all the wave energy at the other end of the tank, the numerical beach. In the current model, in order to reduce the size of the computational domain, an active wave absorption method is employed. At the downstream boundary, waves opposite to the reflected waves are generated, achieving a net cancellation of the wave energy at the end of the domain. A horizontal velocity following the shallow water theory is prescribed (Schäffer and Klopman, 2000) on the downstream boundary.

$$U(t) = -\sqrt{\frac{g}{d}}\,\xi(t) \tag{5}$$

$$\xi(t) = \eta(t) - d \tag{6}$$

Here, $\eta(t)$ is the actual free surface location along the downstream boundary and d the water depth.

Numerical evaluation of wave forces

The total breaking wave forces on a cylinder are calculated by integrating the pressure p and the surface normal component of the viscous shear stress tensor τ on the surface of the solid objects as follows:

$$F = \int_{\Omega} (-\mathbf{n}p + \mathbf{n}\cdot\tau) d\Omega \tag{7}$$

where **n** is the unit normal vector pointing into the fluid and Ω is the surface of the object.

RESULTS

Validation: Breaking wave force on a single cylinder

The breaking wave forces on a single vertical cylinder are calculated and compared to experimental data from the experiments were carried out at the Large Wave Flume (GWK), Hannover, Germany (Irschik *et al.*, 2002). The cylinder has a diameter $D = 0.7$ m, placed in a water depth of $d = 3.80$ m. Regular waves of period $T = 4.0$ s and height $H = 1.30$ m are incident on the cylinder that is placed at the crest of a 23 m long 1 : 10 slope. The still water depth at the cylinder is $d = 1.50$ m in the experimental setup.

In the numerical setup the wave tank is 56 m long, 5 m wide and 7 m high. A grid size of $dx = 0.05$ m is used, resulting in a total of 15.68 million cells. A cylinder with $D = 0.7$ m is placed at the crest of a 23 m long 1 : 10 slope, with its centre at 44.0 m with the incident waves of period $T = 4.0$ s breaking exactly on the front surface of the cylinder. The numerical setup is illustrated in Fig. (1), where except for the total length of the tank, the other conditions are similar to the experimental setup. Further details regarding the numerical setup can be obtained in Kamath *et al.* (2016).

The numerically calculated wave force is compared to the EMD (Empirical Mode Decomposition) treated experimental data from Choi *et al.* (2015) to filter out the dynamic amplification of the wave forces due to the vibration of the cylinder in Fig. (2). A good agreement is seen between the numerical and experimental breaking wave forces on a single vertical cylinder.

Breaking wave force on tandem cylinders

The breaking wave interaction with a single vertical cylinder results in several distinct free surface features such as the separation of the breaking wavefront around the cylinder, the subsequent meeting of the separated wave front and the formation of a water jet downstream of the cylinder. These features have been presented and discussed by Kamath *et al.* (2016). Here, the effect of the free surfaces features from breaking wave interaction with the upstream cylinder on the hydrodynamics of a cylinder placed downstream is studied in different scenarios: when the wave breaking point is on the surface of the upstream cylinder and when the wave breaking point is just behind the upstream cylinder. For each of the breaking scenarios, the distance between the two cylinders is varied and the effect on the breaking wave forces on the downstream cylinder is investigated.

Breaking point on the front surface of the upstream cylinder

In this scenario, the wave breaking point is on the surface of the upstream cylinder and the downstream cylinder is placed at distances of $S = 1D$, $2D$, $3D$, $4D$ and $5D$ from the upstream cylinder. The breaking wave force on a single cylinder in this scenario is 13900 N. The variation of the total breaking wave force on the downstream cylinder with the distance of the downstream cylinder from the upstream cylinder is presented in Fig. (3).

The wave force on the downstream cylinder is seen to increase as the distance between the cylinders is increased from $S = 1D$ to $3D$. At a centre-to-centre distance of $S = 3D$, the force on the downstream cylinder is seen to be the maximum under this scenario of wave impact. A further increase in the distance between the cylinders results in a decrease in the total breaking wave force. At a centre-to-centre distance of $S = 5D$, the total breaking wave force on the downstream cylinder is similar to that at $S = 1D$.

The variation of the total breaking wave forces on the downstream cylinder is a consequence of the free surface features associated with the breaking wave interaction with the upstream cylinder and the resulting wave incident on the downstream cylinder. The downstream cylinder is within the shadow region of the upstream cylinder at a separation distance of $S = 1D$. Here, the overturning wave crest incident on the upstream cylinder with a vertical wavefront gets separated around the upstream cylinder. The downstream cylinder is then in the shadow zone and impacted by a smaller mass of water compared to the upstream cylinder. This leads to smaller breaking wave forces on the downstream cylinder. As the separation distance is increased, the downstream cylinder moves out side the shadow region. The cylinder is then impacted by a larger mass of water formed by the rejoining of the separated wavefront, downstream of the first cylinder. This results in increasing total breaking wave forces on the downstream cylinder, with a maximum seen for $S = 3D$.

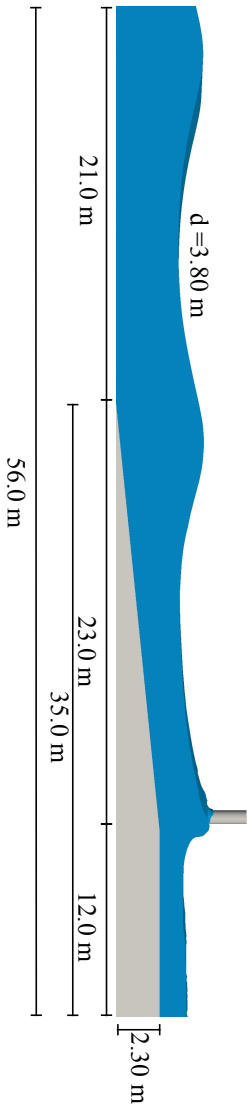

Figure 1: Numerical setup used for investigate breaking wave forces on a cylinder

As the separation distance is further increased beyond $S = 3D$, the downstream cylinder is outside the shadow region, but now impacted by the splash up from the overturned wave crest. With increasing distance from this point onwards, the total breaking wave force on the downstream cylinder is reduced.

The free surface features associated with breaking wave interaction with a pair of tandem cylinders placed with a separation distance $S = 2D$ is presented in Fig. (4). The incident wave on the upstream cylinder, impacting the cylinder with a vertical wave front crest is seen in Fig. (4a). The separation of the wavefront around the upstream cylinder as the incident wave crest begins to overturn is shown in Fig. (4b). The downstream cylinder is in the shadow zone in Fig. (4c), where the overturning wave crest impacts the cylinder with significantly smaller mass of water due to the separation of the wavefront around the upstream cylinder. Fig. (4d) shows the overturned wave crest after it passes the downstream cylinder and the runup on the downstream cylinder due to the water jet formed behind the upstream cylinder.

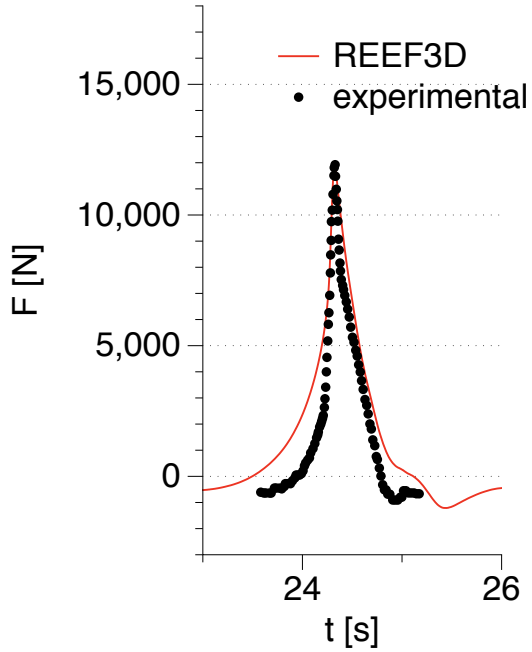

Figure 2: Comparison on numerical and experimental breaking wave forces on the single cylinder

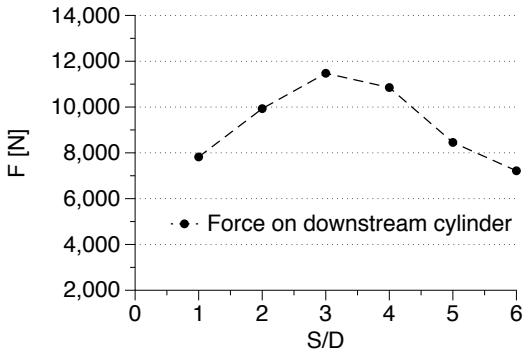

Figure 3: Variation of the breaking wave forces on the downstream cylinder with increasing distance from the upstream cylinder when the wave breaks on the surface of the upstream cylinder

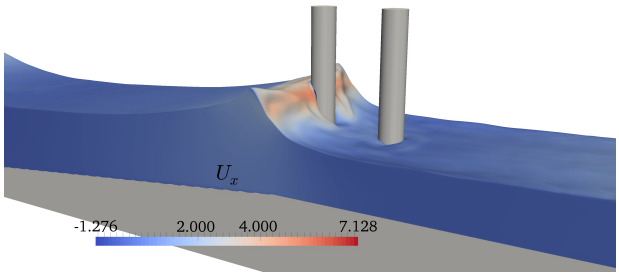

(a) $t/T = 3.40$

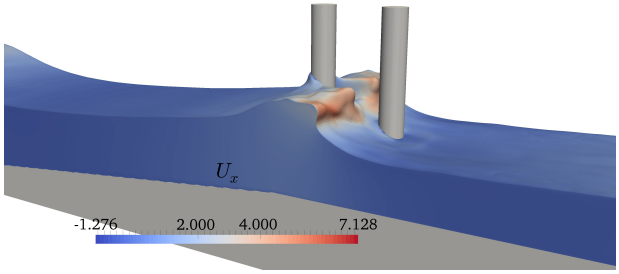

(b) $t/T = 3.70$

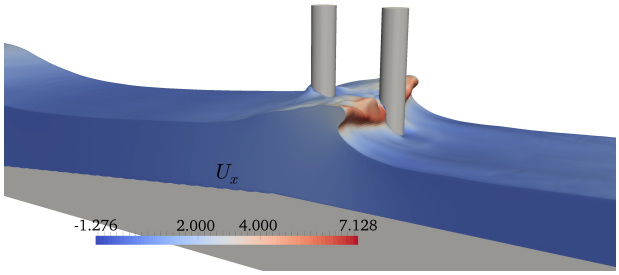

(c) $t/T = 3.85$

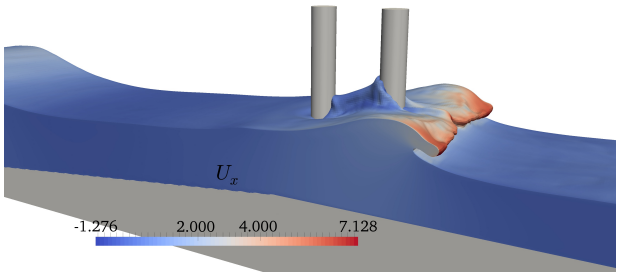

(d) $t/T = 4.25$

Figure 4: Breaking wave interaction with tandem cylinders placed with a distance of $2D$ between their centers, with the wave breaking point on the surface of the upstream cylinder

At a separation distance of $S = 4D$, the downstream cylinder is outside the shadow region of the upstream cylinder. The vertical incident wave crest front on the upstream cylinder in this case is presented in Fig. (5a). The separation of the overturning wave crest around the upstream cylinder and the development of the plunger are seen in Figs. (5b) and (5c) respectively. Fig. (5d) shows the impact of the overturned wave crest on the downstream cylinder. The downstream cylinder is outside the shadow region behind the upstream cylinder, but is impacted by the plunger before it reconnects with the

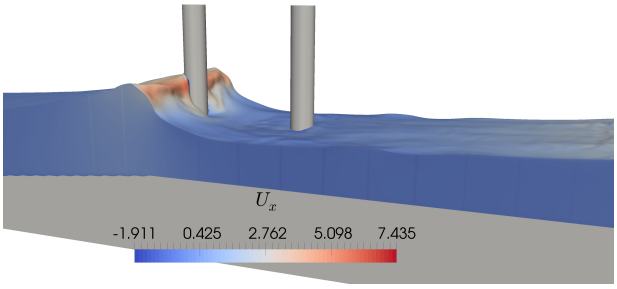

(a) $t/T = 3.40$

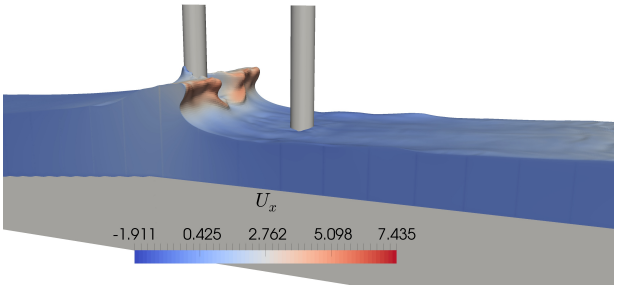

(b) $t/T = 3.65$

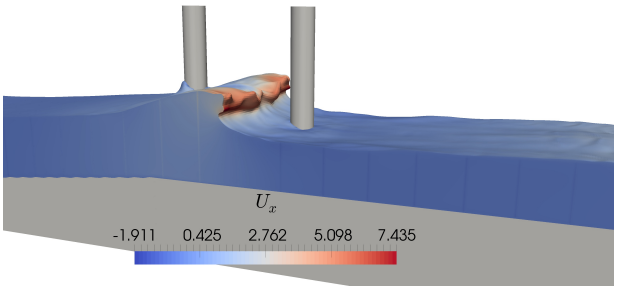

(c) $t/T = 3.90$

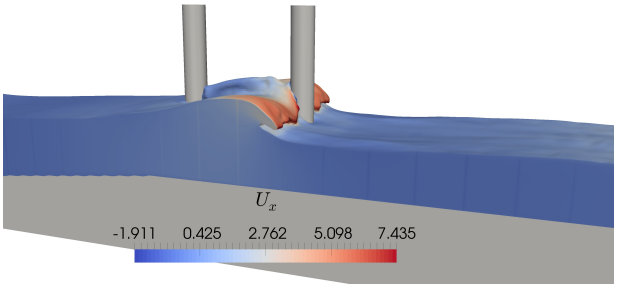

(d) $t/T = 4.15$

Figure 5: Breaking wave interaction with tandem cylinders placed with a distance of $4D$ between their centres, with the wave breaking point on the surface of the upstream cylinder

preceding wave crest. While the breaking wave forces on the downstream cylinder in this case are lower than than for $S = 3D$, they are higher than for $S = 1D$ and $2D$. In the case of $S = 3D$, the plunger would impact the cylinder just under the wave crest level and thus result in the highest wave force on the cylinder in this scenario of wave impact, following Irschik *et al.* (2002), Irschik *et al.* (2004) and Kamath *et al.* (2016).

Breaking point behind the upstream cylinder

In this scenario, the wave breaking point is just behind the upstream cylinder and the downstream cylinder is placed at distances of $1D$, $2D$, $3D$, $4D$ and $5D$ from the upstream cylinder. The breaking wave force on a single cylinder in this scenario is 9800 N. Fig. (6) shows the variation of the total breaking wave forces on the downstream cylinder with the distance between the two cylinders in this scenario. In this scenario of wave impact, the total breaking wave forces on the downstream cylinder are seen to increase with increasing separation distance S, until $S = 5D$. Further increase in S results in a reduction in the breaking wave force.

The variation of the total breaking wave force on the downstream cylinder seen in Fig. (6) is justified as follows. As the wave breaking point is behind the upstream cylinder, the downstream cylinder is effectively in direct exposure to the breaking wave impact. With increasing S, the downstream cylinder is placed in positions which result in higher total breaking wave forces. According to the results presented by Irschik *et al.* (2004) and Kamath *et al.* (2016), the total breaking wave forces on a single vertical cylinder are the highest when the overturning wave crest impact the cylinder just below the wave crest level followed by wave impact around crest level and vertical impact. From the results for breaking wave interaction with cylinders placed in tandem, similar conclusions can be drawn.

The breaking wave interaction with the tandem cylinders placed with a separation distance of $S = 1D$ is presented in Fig. (7). The wave incident on the upstream cylinder is yet to obtain a vertical wave crest front in Fig. (7a). The incident wavefront is separated around the upstream cylinder and attains a vertical wave crest front profile just passing the cylinder in Fig. (7b). The impact of the overturning wave crest on the downstream cylinder is seen in Fig. (7c). Here, the impacting overturning wave crest is still separated and thus the wave impact on the downstream cylinder is by a lower mass of water, resulting in the lowest breaking wave forces in this scenario. The runup on the downstream cylinder as the overturning wave crest passes the downstream cylinder is seen in Fig. (7d).

In the case of separation distance $S = 5D$, the total breaking wave forces on the downstream cylinder are the maximum in this scenario of breaking wave impact. Fig. (8a) shows the wave incident on the upstream cylinder which has not yet attained a vertical wave crest front. The incident wave is separated and attains a vertical wave crest front in

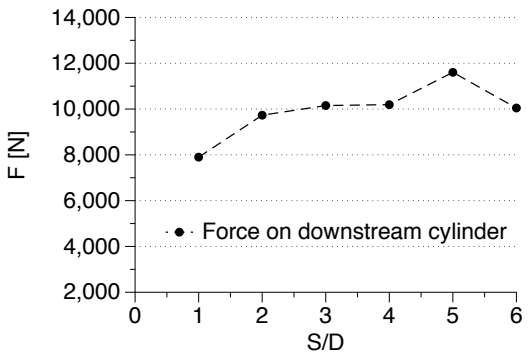

Figure 6: Variation of the breaking wave forces on the downstream cylinder with increasing distance from the upstream cylinder when the wave breaks just behind the upstream cylinder

Fig. (8b) as it passes the upstream cylinder. The overturning wave crest propagating between the two cylinders is seen in Fig. (8c). Finally, the impact of the overturning wave crest on the downstream cylinder, just below the wave crest level is seen in Fig. (8d). Thus, in this impact scenario where the wave breaking point is just behind the upstream cylinder, the wave forces on the downstream cylinder increase with increase in S, due to the cylinder moving away from the shadow zone and being exposed to the overturning wave crest under conditions of impact that result in higher total breaking wave forces.

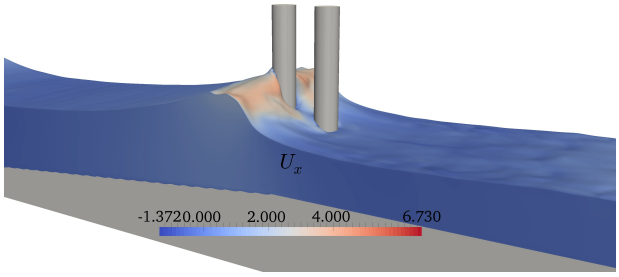

(a) $t/T = 3.20$

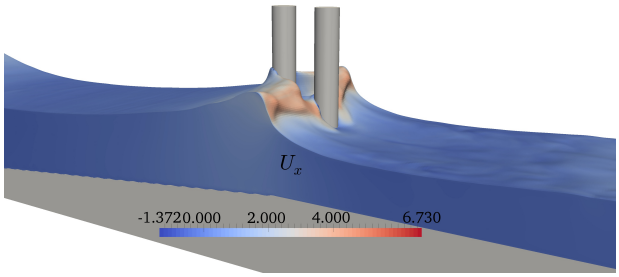

(b) $t/T = 3.40$

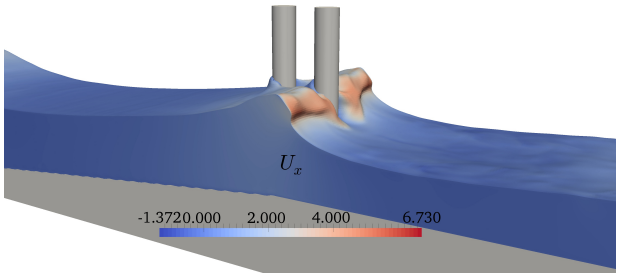

(c) $t/T = 3.55$

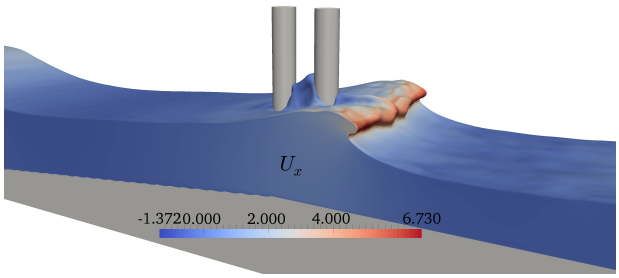

(d) $t/T = 3.90$

Figure 7: Breaking wave interaction with tandem cylinders placed with a distance of $1D$ between their centers, with the wave breaking point just behind the upstream cylinder

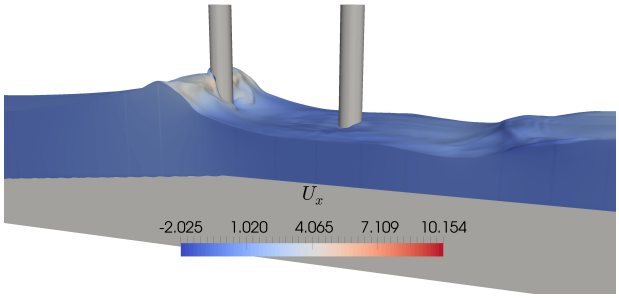

(a) $t/T = 3.20$

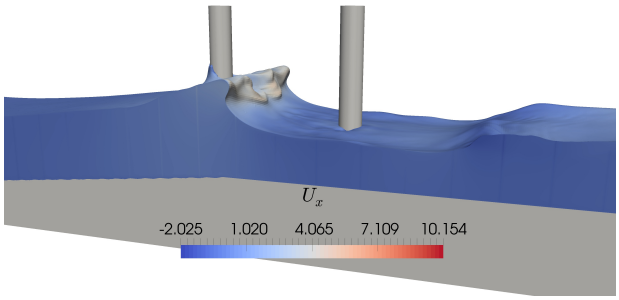

(b) $t/T = 3.45$

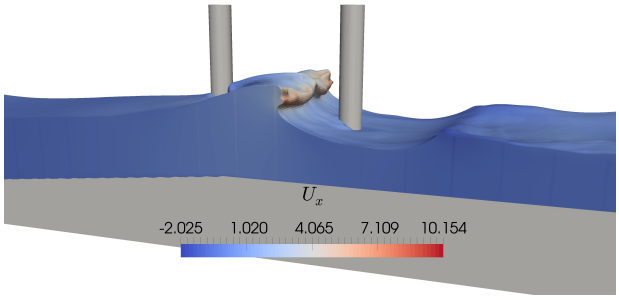

(c) $t/T = 3.80$

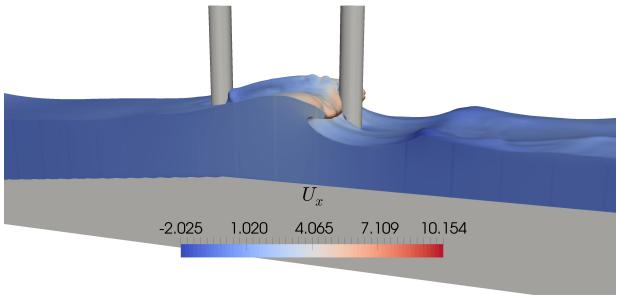

(d) $t/T = 4.00$

Figure 8: Breaking wave interaction with tandem cylinders placed with a distance of $5D$ between their centres, with the wave breaking point just behind the upstream cylinder

CONCLUSION

The conclusions are:

1. Breaking wave forces on the downstream cylinder in a tandem arrangement follow a similar trend as that observed for a single cylinder, with maximum breaking wave forces calculated for the case where the overturning wave crest impacts the cylinder just below the wave crest level.

2. The free surface features due to breaking wave interaction with the upstream cylinder such as the separation of

the wavefront, rejoining of the separated wavefront and the formation of the water jet influence the wave forces on the downstream cylinder.

3. The shadow zone behind the upstream cylinder is less than $3D$ for vertical wave crest impact on the upstream cylinder, while it is about $1D$ for wave breaking just behind the upstream cylinder.

4. The breaking wave force on the downstream cylinder can be equal to or higher than the breaking wave force on a single cylinder under certain arrangements.

REFERENCES

(2015). *HYPRE high performance preconditioners - User's Manual*. Center for Applied Scientific Computing, Lawrence Livermore National Laboratory.

ALAGAN CHELLA, M., BIHS, H., MYRHAUG, D. and MUSKULUS, M. (2015a). "Breaking characteristics and geometric properties of spilling breakers over slopes". *Coastal Engineering*, **95**, 4–19.

ALAGAN CHELLA, M., BIHS, H. and MYRHAUG, D. (2015b). "Characteristics and profile asymmetry properties of waves breaking over an impermeable submerged reef". *Coastal Engineering*, **100**, 26–36.

ALAGAN CHELLA, M., BIHS, H., MYRHAUG, D. and MUSKULUS, M. (2015c). "Hydrodynamic characteristics and geometric properties of plunging and spilling breakers over impermeable slopes". *Ocean Modelling, Virtual Special Issue: Ocean Surface Waves*, 1–20.

ASHBY, S.F. and FLAGOUT, R.D. (1996). "A parallel mulitgrid preconditioned conjugate gradient algorithm for groundwater flow simulations". *Nuclear Science and Engineering*, **124(1)**, 145–159.

BERTHELSEN, P.A. and FALTINSEN, O.M. (2008). "A local directional ghost cell approach for incompressible viscous flow problems with irregular boundaries". *Journal of Computational Physics*, **227**, 4354–4397.

BIHS, H., KAMATH, A., ALAGAN CHELLA, M., AGGARWAL, A. and ARNTSEN, Ø.A. (2016). "A new level set numerical wave tank with improved density interpolation for complex wave hydrodynamics". *Computers & Fluids*, **140**, 191–208.

BREDMOSE, H. and JACOBSEN, N.G. (2010). "Breaking wave impacts on offshore wind turbine foundations: focused wave groups and CFD". *Proc., 29th International Conference on Ocean, Offshore and Arctic Engineering, Shanghai, China*.

CHOI, S.J., LEE, K.H. and GUDMESTAD, O.T. (2015). "The effect of dynamic amplification due to a structureŒş s vibration on breaking wave impact". *Ocean Engineering*, **96**, 8–20.

CHORIN, A. (1968). "Numerical solution of the Navier-Stokes equations". *Mathematics of Computation*, **22**, 745–762.

DURBIN, P.A. (2009). "Limiters and wall treatments in applied turbulence modeling". *Fluid Dynamics Research*, **41**, 1–18.

IRSCHIK, K., SPARBOOM, U. and OUMERACI, H. (2002). "Breaking wave characteristics for the loading of a slender pile". *Proc. 28th International Conference on Coastal Engineering, Cardiff, Wales*.

IRSCHIK, K., SPARBOOM, U. and OUMERACI, H. (2004). "Breaking wave loads on a slender pile in shallow water". *Proc. 29th International Conference on Coastal Engineering, Lisbon, Portugal*.

JACOBSEN, N.G., FUHRMAN, D.R. and FREDSØE, J. (2012). "A wave generation toolbox for the open-source CFD library: OpenFOAM". *International Journal for Numerical Methods in Fluids*, **70(9)**, 1073–1088.

JIANG, G.S. and SHU, C.W. (1996). "Efficient implementation of weighted ENO schemes". *Journal of Computational Physics*, **126**, 202–228.

KAMATH, A., ALAGAN CHELLA, M., BIHS, H. and ARNTSEN, Ø.A. (2016). "Breaking wave interaction with a vertical cylinder and the effect of breaker location". *Ocean Engineering*, **128**, 105–115.

LARSEN, J. and DANCY, H. (1983). "Open boundaries in short wave simulations - a new approach". *Coastal Engineering*, **7**, 285–297.

LIN, P. and LIU, P.L.F. (1998). "A numerical study of breaking waves in the surf zone". *Journal of Fluid Mechanics*, **359**, 239–264.

MO, W., JENSEN, A. and LIU, P.L.F. (2013). "Plunging solitary wave and its interaction with a slender cylinder on a sloping beach". *Ocean Engineering*, **74**, 48–60.

NAOT, D. and RODI, W. (1982). "Calculation of secondary currents in channel flow". *Journal of the Hydraulic Division, ASCE*, **108(8)**, 948–968.

OSHER, S. and SETHIAN, J.A. (1988). "Fronts propagating with curvature- dependent speed: algorithms based on Hamilton-Jacobi formulations". *Journal of Computational Physics*, **79**, 12–49.

SCHÄFFER, H.A. and KLOPMAN, G. (2000). "Review of multidirectional active wave absorption methods". *Journal of Waterway, Port, Coastal, and Ocean Engineering*, **126(2)**, 88–97.

SHU, C.W. and OSHER, S. (1988). "Efficient implementation of essentially non-oscillatory shock capturing schemes". *Journal of Computational Physics*, **77**, 439–471.

VAN DER VORST, H. (1992). "BiCGStab: A fast and smoothly converging variant of Bi-CG for the solution of nonsymmetric linear systems". *SIAM Journal on Scientific and Statistical Computing*, **13**, 631–644.

WILCOX, D.C. (1994). *Turbulence modeling for CFD*. DCW Industries Inc., La Canada, California.

ZHAO, Q., ARMFIELD, S. and TANIMOTO, K. (2004). "Numerical simulation of breaking waves by a multi-scale turbulence model". *Coastal Engineering*, **51(1)**, 53–80.